

interferometer. The sample arm of the interferometer comprises of a fiber collimator lens, polariser, an electro-optic polarization modulator (PM), a galvo-scanner mirror, and an objective lens. The PM was used to illuminate the sample with desired incident polarizations. We employed in the reference arm of the interferometer, an optical arrangement, similar to the Fourier domain optical delay line in order to minimize the dispersion mismatch in the interferometer. Three different polarization states of light were used to illuminate the sample sequentially. For each incident polarization, the light back-reflected from both the reference and sample arms is collected by a 50/50 coupler and coupled to an InGaAs balanced photo receiver. The interferometric signal was digitized using a high-speed data acquisition board (NI-5122). The measured interferogram signal was processed (wave number-resampling, dispersion compensation, FFT) to provide the depth resolved reflectivity, birefringence and optic axis orientation profile of the sample. LabView based software was developed to control the entire setup and for signal processing along with image display. The signal to noise ratio (SNR) of the setup was  $\sim 95$  dB. The axial and lateral resolutions of the setup were  $\sim 12 \mu\text{m}$  and  $\sim 30 \mu\text{m}$  (with a 5X objective lens in sample arm) respectively. The imaging speed of the setup was  $\sim 6$  frames per second (fps) for OCT intensity images and  $\sim 2$  fps for PSOCT images.

For calibration of the SS-PSOCT setup, the retardance of a quarter wave plate was measured for different orientations (from  $0^\circ$  to  $360^\circ$  in steps of  $10^\circ$ ) of its fast axis in a plane perpendicular to the light path. The average retardation value for  $0^\circ$  to  $360^\circ$  fast axis orientation was measured to be  $176.5^\circ$  with standard deviation  $2.5^\circ$ . The setup has also been used to obtain intensity, retardation and fast axis orientation images of the nail fold of a healthy human volunteer in-vivo (Fig. L.5.2).

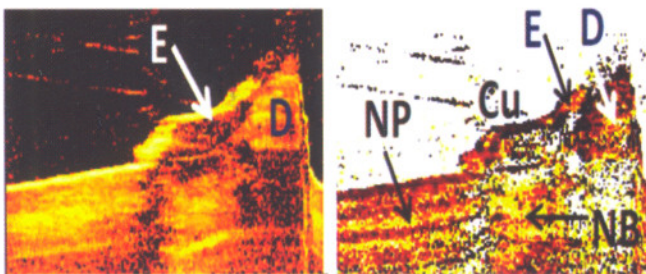


Fig.L.5.2. Intensity (left) and retardation (right) images of human nail fold. Cu: cuticle; D: dermis; E: epidermis; NB: nail bed; NP: nail plate; Image dimensions are 3mm (lateral)  $\times$  2mm (depth).

In summary, we have demonstrated a single detector based fiber-optic PSOCT scheme using a swept laser source for generating intensity, retardation and optic axis orientation images of biological tissues. With the rapid advances in swept source technology both in terms of the line rate and miniaturization, this scheme may find potential clinical

applications for volumetric polarization sensitive imaging compared to the conventional intensity based data.

Reported by:

P. Sharma, Y. Verma, K. Divakar Rao  
(kdivakar@rrcat.gov.in) and P. K. Gupta

## L.6: Orientation and rotation of red blood cells with Laguerre-Gaussian trap beams

Red blood cells (RBCs) have a discotic shape and when optically trapped the cell orients itself in a side on or vertical configuration. Earlier we have developed methods for controlling the stable orientation of the trapped cells using either a combination of point and line tweezers or combination of cw and pulsed trap beams. Such control on orientation has important applications in recording polarized Raman spectra from optically trapped RBCs. Recently we carried out experiments at Laser Biomedical Applications and Instrumentation Division to explore the possibility of using Laguerre-Gaussian (LG) trap beam instead of conventional  $\text{TEM}_{00}$  trap beam to control the orientation of trapped RBCs. Further, since LG trap beams have orbital angular momentum associated with their helical wavefronts, experiments were also carried out to investigate use of these beams to rotate trapped RBCs. Such use of RBCs as micro-rotor has potential applications in microfluidics.

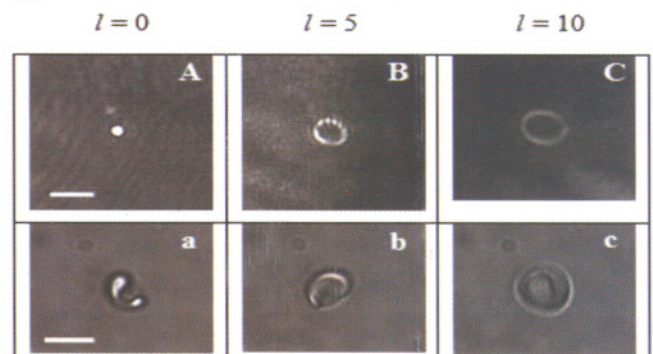


Fig.L.6 1: Trapping LG beam profiles for topological charges 0, 5 and 10 (A-C) and the corresponding orientation of a trapped RBC (a-c) respectively. Scale bar, 2.5  $\mu\text{m}$ . (A-C) and 6  $\mu\text{m}$  (a-c).

The LG modes have an annular intensity profile, size of which increases with the azimuthal index or topological charge of the mode. We observed that control over the orientation of the trapped RBC in the vertical plane could be achieved with a change in the topological charge of the trapping beam. Fig. L.6.1 shows the change in the orientation of a trapped RBC with changes in the topological charge of the LG modes. For the zeroth order LG mode (which is identical to  $\text{TEM}_{00}$ ) the cell orients with its plane along the direction of the

trapped beam (vertical orientation), since this maximizes the overlap of the cell volume with the region of highest light field. As the size of the bright annulus increases with mode order, maximum overlap between the cell volume and the trapping field is expected for cell orientation away from the vertical direction. For  $l=10$  the cell can be seen to be oriented in the horizontal plane that is the trapping plane as this maximizes the overlap of the cell volume with the region of highest light field.

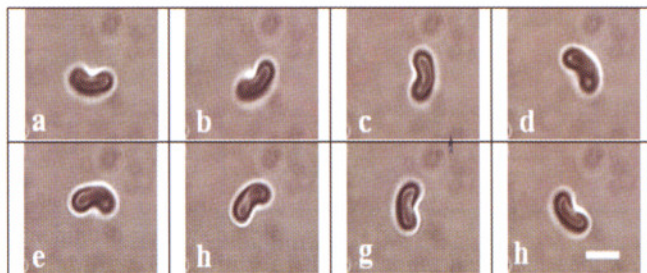


Fig. L.6.2. The rotation of a trapped RBC via transfer of light orbital angular momentum when trapped under  $l=15$  mode. In (a)-(h) the cell is observed to be rotated by an angle of  $45^\circ$  over the previous frame. The time separation between the frames is  $\sim 625$  ms. Scale bar,  $5 \mu\text{m}$ .

We also observed that the torque exerted by LG trapping beam with high topological charges ( $|l| \sim 15$  or more) could drive RBCs as natural micro-rotors. For  $|l| \sim 15$  the trapped cells get aligned over the bright annulus of the LG trap due to larger circumference of the annulus. Under such condition the cells while being contained within the annular ring of light, orbits the beam axis in a direction determined by the handedness of the helical phase fronts. This is believed to be due to the transfer of light orbital angular momentum to the trapped cells by the scattering of the trap beam having helical wavefront. Fig. L.6.2 shows the rotation of an RBC when trapped under  $l=15$  mode. The observed rotational frequency was  $\sim 12$  rpm at  $\sim 15$  mW of trapping power and it can be increased using higher trap beam power. To check whether the observed rotation is caused by the transferred light orbital angular momentum from the trap beam to the cell we changed the helicity of the trap beam. The sense of rotation was observed to get reversed as the charge of the LG mode was made negative. This allows for a means to change the sense of rotation of a micro-rotor system by simply changing the helicity of the trapping beam. Such control over rotational sense is not possible with techniques utilizing specially fabricated micro-structures or RBCs suspended in hypertonic buffers. A control on the sense of rotation can facilitate bi-directional operation for micro-machine components like micro-motors or valves.

Reported by:

R. Dasgupta (raktim@rrcat.gov.in), S. Ahlawat,  
R. S. Verma and P. K. Gupta

## L.7: 5 kW CW CO<sub>2</sub> Laser for Material Processing

A 5 kW CW CO<sub>2</sub> laser system was developed long back in LMPD. With time, various problems concerned in performance of high power CW CO<sub>2</sub> laser viz. rapid decrease in beam shape & size and laser power, short gas lifetime, electrode deposits, fast degradation of cavity mirrors and frequent replacement/maintenance of laser sub-systems were recorded. Therefore, the existing 5 kW CW CO<sub>2</sub> laser system has been renovated to overcome these problems and improve its performance. Various modifications in design of laser sub-systems have been done. All the mechanical sub-systems, except vacuum chamber, vacuum pump and SMPS; were redesigned, procured and assembled. The major modified components of laser system are various subassemblies viz blowers, gas flow loop, electrodes, resonator, coolant circuit etc. Some of the important modifications made in the laser system (Fig.L.7.1) are described below.



Fig.L.7.1: Renovated 5kW CW CO<sub>2</sub> laser

Corrosion of blower housing, motors, ducts and supporting structure have been minimized through suitable choice of materials.

Belt drive of blower is replaced with direct drive to eliminate debris from belt and pulley drive.

In the electrode assembly, epoxy, araldite and PVC tubing are replaced with high temperature materials to minimize degradation from discharge-induced UV radiation.

All four cavity mirrors are mounted on a single resonator structure to minimize cavity misalignment.

A secondary coolant circuit (Fig. L.7.2A) has been introduced to eliminate contamination from other laser systems.

A gas purging system, consisting of purging controller (Fig.L.7.2B), gas cylinder bank and gas changeover, has been introduced for long-term laser operation.

- Flow monitor-cum-switches have been introduced for safety interlocking to prevent accidental switching on of laser system without coolant.
- A pneumatically operated beam shutter-cum-beam dump has been added.